Polarization-independent tunable optical filters based on bilayer polarization gratings

Elena Nicolescu and Michael J. Escuti

North Carolina State Univ, Dept Electrical & Computer Engineering, Raleigh, NC (USA)

ABSTRACT

We report enhanced polarization-independent tunable optical filters based on liquid crystal (LC) and reactive mesogen (RM) polarization gratings (PGs). This new design achieves tunable passbands with significantly smaller bandwidth and allows for potential applications in spectroscopy and beyond. Analogous to Lyot and Solc filters, our filter is constructed of multiple bilayer polarization gratings (BPGs) of varying thicknesses, with the potential for highly compact implementation. BPGs are a hybrid of a switchable/tunable liquid crystal (LC) PG and a reactive mesogen (RM) PG. By adding the RM layer, the BPG provides a significant advantage over LCPGs for the filter application in that it allows very thick gratings to be created with thin active LC layers. As such, the difficulty in fabricating LCPGs with arbirtrarily large thicknesses is much less of a concern. BPGs exhibit the unique properties of PGs, including polarization independent zero-order transmittance, as well as diffraction at visible and infrared wavelengths. Our unique design enables a high peak transmittance ($\sim 90\%$) as well as a significantly improved full-width-at-half-maximum (FWHM). Here, we present preliminary data, discuss the unique capabilities and compelling advantages of our filter. We analyze performance in terms of finesse, 3dB bandwidth (FWHM), and free-spectral-range by comparison to theoretical simulation.

Keywords: liquid crystals, tunable optical filter, bandpass, polarization gratings, diffraction, polarization-independent

1. INTRODUCTION

Tunable optical filters have a very wide range of applications from spectroscopy to optical communication networks, to remote sensing as well as biomedical imaging and diagnostics. In recent years research efforts have focused on miniaturizing tunable optical filters into physically small packages for applications such as compact portable spectroscopy and hyperspectral imaging for real-time or in-vivo medical diagnostics, or surveillance and defense applications. Previous filter implementations including dispersive elements matched with aperture-stops (Czerny-Turner), mechanically tuned etalons (Fabry-Perot), and assemblies of stacked birefringent waveplates and polarizers (Lyot, Solc, and Evans) are not ideal for these applications due to high cost of implementation, high insertion losses, strong polarization sensitivity, or difficulty in miniaturization. In this work we introduce the Bilayer Polarization Grating (BPG), a novel diffractive optical element, which enables the implementation of a tunable optical filter completely insensitive to input polarization and exhibiting high peak transmittance and a potential for very low cost and compact implementation. We will first consider the theory and fabrication of the BPG itself, highlighting its compelling properties and unique advantages for the tunable filter application. We will then demonstrate two configurations of a tunable optical filter based on BPGs and analyze it in terms of key filter parameters including bandwidth, *finesse*, free-spectral-range, peak transmittance, and maximum tuning range.

2. BACKGROUND

2.1 Tunable Optical Filters and Applications

The applications of tunable optical filters are many and varied ranging from astronomy to medicine, education, remote-sensing, optical communications and even the cosmetics industry. The broader application area, which encompasses most of the above, is spectroscopy or hyperspectral imaging. Specifically compact spectroscopy and

Correspondence should be addressed to: mjescuti@ncsu.edu, +1 919 513 7363

Liquid Crystals XII, edited by Iam Choon Khoo, Proc. of SPIE Vol. 7050, 705018, (2008)
0277-786X/08/$18 · doi: 10.1117/12.795679

hyperspectral imaging applications have been the topic of much research in recent years. The following discussion will give a brief overview of current compact tunable optical filter technologies as they pertain to applications in (imaging) spectroscopy.

The most successful compact spectrophotometer designs demonstrated include the Czerny-Turner,[1,2] Fabry-Perot,[3,4] Lyot-type[5,6] and even MEMS[2] based configurations. The Czerny-Turner configuration is one of the more common designs for spectrophotometers. This system is based on a diffraction grating that separates the wavelengths which are then detected using a CCD array. The main disadvantage of this design is that it is dependent on spatial dispersion thereby causing decreased resolution with increased miniaturization.

Tunable Fabry-Perot etalon filters have also been used in portable spectroscopy. Traditionally, these are made of two highly reflective mirrors separated by a distance which, along with the refractive index of the material between the plates, determines the *finesse* of the filter. The cavity may be filled with nematic liquid crystal which allows the filter to be tuned by applying voltage instead of changing the distance between the plates.[7] Although this design boasts a wide free spectral range and tunable range, high resolution, and low driving voltage, its main disadvantage is that it requires the use of polarizers in order to pass the tunable mode of light and block the non-tunable mode. A reduced polarization dependence has also been achieved by the addition of birefringent quarter waveplates[4] in an optical fiber-based scheme.

Optical bandpass/notch filters have been implemented using stacked birefringent layers. Traditional Lyot-Ohman,[5,8] Solc[9–11] , and Evans[12] filters are composed of a series of birefringent plates and polarizers. In order to achieve electrical tunability, the traditional birefringent plates can be replaced with a series of variable liquid crystal waveplates.[13] The primary disadvantage of such systems is their dependence on polarizers, which significantly increases signal loss and which are difficult/costly to implement at wavelengths outside the visible range.

LC tunable reflection filters have been demonstrated by manipulating the unique properties of cholesteric LCs. For instance, in chiral nematics, an electric field applied perpendicular to the helical axis can deform the chiral pitch and shift the reflected wavelength.[14] While this approach avoids polarizers, it only operates on a single circular polarization handedness and its passband peak reflectance has an inherently strong voltage-dependency. In an alternative approach, a vertically-aligned deformed-helix ferroelectric LC can be configured so that a reflective notch filter (via a Bragg effect) can be tuned by temperature[15] and applied voltage.[16] This results in a polarization-independent effect over a wide range, but its notch depth is much less than 100% and has a peak reflectance that varies substantially when tuned (both effects introducing loss in the detected signal).

A basic hyperspectral imaging system consists of a wavelength-tunable imaging optic and a two-dimensional detection array to gather intensity data over a continuous wavelength range for every pixel of the detection array. Here, the tunable optical filter is critical to overall system properties. Researchers have implemented such systems with acousto-optic tunable filters,[17] liquid-crystal tunable optical filters,[18] as well as the push-broom[19] scanning system.

The pushbroom system is, broadly, the hyperspectral counterpart of the Czerny-Turner configuration described in the previous section, and suffers from similar disadvantages. The system depends on spatial dispersion of wavelengths as well as mechanical scanning to collect two-dimentional data. The approach is bulky, requires very careful alignment, and accurate control of moving parts.[19] Acousto-optic and liquid-crystal tunable filters both have an advantage in that they contain no moving parts. However, as with all of the birefringent filter configurations described in the previous section, they are still dependent on polarizers which significantly increase signal loss.

2.2 Polarization Gratings

Polarization gratings[20–22] (PGs), sometimes called anisotropic or vectorial gratings, are embodied as a spatially varying birefringence and/or dichroism, and essentially operate by periodically modulating the polarization state of the wavefront passing through them (as opposed to modulating phase or amplitude alone). One of the most important PG profiles is a continuous, in-plane, linear birefringence texture[23] with a uniaxial optical anisotropy that follows the spatial profile $\mathbf{n}(x) = [\sin(\pi x/\Lambda), \cos(\pi x/\Lambda), 0]$, where Λ is the grating period. These gratings can be created in two varieties, switchable[24,25] and non-switchable[26] (polymer).

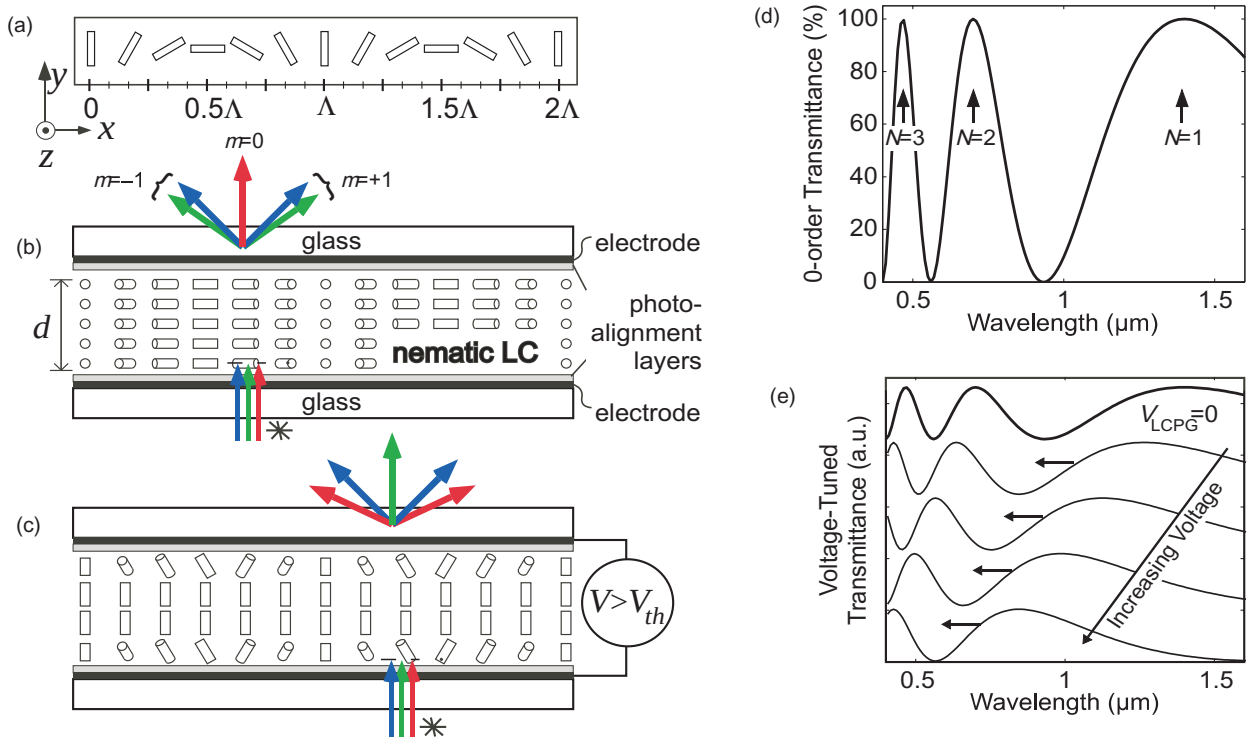

Figure 1. Structure and properties of the liquid crystal polarization grating (LCPG): (a) Basic structure (top view); (b) Basic structure (side view) and illustrated diffraction behavior when $\Delta nd=$ red wavelength with zero applied voltage - note that only the ± 1-orders are ideally present regardless of input polarization; (c) Diffraction behavior when the applied voltage exceeds V_{th} - note that light at different wavelengths couple into the zero-order; (d) Example spectrum ($\Delta n = 0.2$, $d = 7$ μm) shows multiple spectral fringes N over the visible and near-infrared range; and (e) Effect of applied voltage $V_{switchable}$ on spectrum is a blue-shift. Note that illustrations are not drawn to scale. (color figure)

Switchable PGs, also known as Liquid Crystal Polarization Gratings (LCPGs), can be tuned by applied voltage. These gratings can be created using bulk nematic LCs aligned by photo-alignment surfaces that have been exposed with a polarization hologram, leading to the structure illustrated in Fig. 1(a) and (b) where the linear birefringence is embodied in a nematic director $\mathbf{n}(x)$. Note that the key parameters of an LCPG (Fig. 1) include the grating period Λ, grating thickness d, linear birefringence Δn, average index $\bar{n}$, and voltage threshold V_{th}.

Non-switchable or polymer PGs, also known as Reactive Mesogen Polarization Gratings (RMPGs) exhibit the same properties as switchable gratings except that they are unaffected by applied voltage. These gratings are created by spin-coating thin layers of a Reactive Mesogen mixture on a photo-alignment surface that has been prepared in the same way as for switchable gratings[26,27] . The reactive mesogens are low molecular-weight LCs that can be polymerized to form high-molecular weight structures .[28,29] After each layer is coated, it must then be photopolymerized by UV light to permanently fix the grating structure.

Whether switchable or non-switchable, PGs exhibit the same compelling diffraction properties. Assuming the grating parameter[23] $\rho < 2\lambda^2/\bar{n}\Delta n\Lambda^2$, we can express the relevant diffraction efficiency for light normally incident (within $\pm 20°$):

$$\eta_0(\lambda) = \cos^2\left(\frac{\Gamma}{2}\right) \tag{1}$$

where η_0 is the zero-order diffraction efficiency, $\Gamma = 2\pi\Delta nd/\lambda$ is the retardation, and λ is the vacuum wavelength of incident light. Graphed in Fig. 1(d) using representative parameters ($\Delta n = 0.2$ and $d = 7$ μm), several notable

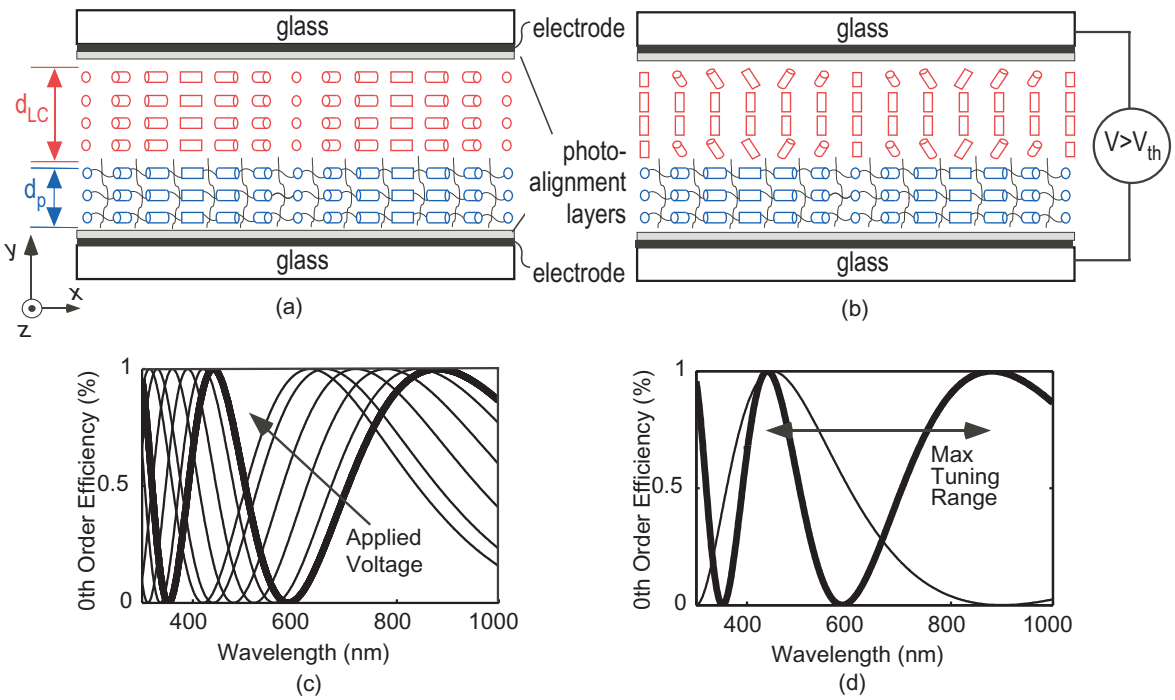

Figure 2. The basic structure and diffraction properties of the BPG: (a) Basic structure (side view) showing the alignment of the switchable and polymer layers; (b) Structure showing the alignment of moleculses with applied voltage; (c) The spectra of a representative BPG where both the polymer and switchable layers are 3 μm thick showing shifting of the peak with applied voltage; (d) Spectra of a BPG showing the maximum tuning range for the condition where both layers are 3μm thick and representative LC birefringence values are chosen (highlighted trend is at 0 voltage and the other is at maximum voltage)

aspects can be observed: (*i*) it can theoretically vary from 100% to 0% depending on the normalized retardation $\Delta nd/\lambda$; (*ii*) the specular transmitted intensity is independent of input polarization and Λ; (*iii*) peak zero-order efficiencies occur at wavelength $\lambda_N = \Delta nd/N$, where N is a non-negative integer corresponding to the spectral fringe; and conversely, (*iv*) the thickness required to arrange a fringe N at a wavelength λ_N obeys the rule

$$d = N\lambda_N/\Delta n. \tag{2}$$

The diffraction efficiency of the switchable gratings can be controlled by applied voltage which decreases the effective birefringence (Δn becomes $\Delta n(V)$ in Eq. 1). An applied external voltage V (Fig. 1(b)) causes the nematic director to reversibly reorient out-of-plane, thereby leading to a blue-shift in the entire spectrum (Fig. 1(e)). For instance, if at 0 applied voltage, green light is transmitted and other wavelengths are diffracted, a small applied voltage (<1-2 V) can cause the cell to transmit blue light and diffract all others. It is important to note here that the voltage threshold to initiate electrical tuning is very modest (<1-2 V) even for very thick gratings.

Previously we introduced a tunable optical filter based on switchable PGs.[30] The main limitation of using these gratings for the filter application is the inability to create high quality LCPGs of arbitrary thicknesses, which are needed in order to optimize key filter parameters including FWHM and *finesse*.

3. BILAYER POLARIZATION GRATING

3.1 BPG Theory

The Bilayer Polarization Grating (BPG) is a novel combination of a switchable PG and a polymer PG with the basic structure shown in Fig. 2(a) and (b). The primary advantage of this structure is allowing for the fabrication

of very thick gratings while maintaining all of the compelling properties of standard switchable PGs. Since the polymer PG is more robust and very thick films can be created with high quality, we use the polymer layer to determine the nominal thickness of the grating and we add only a thin layer of nematic LC to achieve tuning by applied voltage.

The diffraction from the BPG follows the same pattern as that of a traditional LCPG (only zero and first orders are visible) and its zero-order diffraction efficiency is also described by Eq. 1. The primary difference is that in a BPG the retardation (Γ) has to take into account the individual retardation of each layer. The total local retardation is expressed in Eq. 3 where d_P and Δn_P refer to the properties of the polymer layer and d_{LC} and Δn_{LC} refer to the properties of the switchable layer.

$$\Gamma = \frac{2\pi(\Delta n_p * d_p + \Delta n_{LC} * d_{LC})}{\lambda} \tag{3}$$

From this governing equation we extract the most important design parameters. Similar to the LCPG, the zero-order diffraction efficiency peaks occur at wavelengths given by Eq. 4 where N corresponds to the spectral fringe. However, the thickness required to arrange a fringe N at a wavelength λ_n is harder to extract from this equation since we are dealing with two independent thickness variables (one for the polymer layer and one for the LC layer). Therefore in this approach, instead of arranging a specific fringe N to occur at a given wavelength λ_N, we first decide the minimum value of the desired tuning range. This value is set by the birefringence and thickness of the polymer layer as $\lambda_N = \Delta n_P d_P/N$. The maximum limit of the tuning range is then determined by the the birefringence and thickness of the liquid crystal layer as $\lambda_N = \Delta n_S d_S/N$, keeping in mind that a switchable layer greater than $\frac{\Lambda}{2}$ is unlikely to align well just like for standard LCPGs. Fig. 2(c) shows the tuning characteristics of a representative BPG designed with both switchable and polymer layers to be $3\mu m$ where the birefringence of the switchable LC is chosen as 0.1434 and the birefringence of the polymer layer is chosen as 0.15 (note these are representative values of the materials used in our experiments). Fig. 2(d) shows the maximum tuning range of the BPG.

$$\lambda_N = \frac{d_P \Delta n_P + d_S \Delta n_S}{N} \tag{4}$$

3.2 Fabrication

The basic fabrication process of a BPG consists of a combination of the switchable and polymer PG fabrication steps. First, a polarization hologram[20,31] is created by superimposing two coherent beams from an ultraviolet laser with orthogonal circular polarizations with a small angle between them (easily creating periods $\Lambda > 4$ μm). Next, one ITO coated glass substrate is coated with a photoalignment material,[32,33] in this case ROP103-2CP (Rolic Technologies Ltd). The substrate is then exposed to the polarization hologram capturing the pattern in the photo-aigmnment layer[20,24,31] (Fig. 1(a)). The polymer liquid crystal RMS03-001C (Merck) is then spin-coated onto the substrate in thin layers according to the process in Ref.[26] After each layer is applied, it must be photopolymerized by UV lamp. This process is repeated until a polymer layer of the desired thickness is achieved. A second ITO glass substrate is then coated to achieve a degenerate-planar anchoring condition.[34] This is neccessary to improve liquid crystal alignment to this surface which cannot be exposed to the polarization hologram. The two ITO substrates are then laminated together such that a uniform thickness (usually a few μm) is achieved. Finally, a nematic LC (in this case MDA06-177 from Merck) is injected into the cell gap and fills by capillary action. The surfaces direct the LC orientation to create the structure shown in Fig. 2(a). The entire process described above can be summarized in six basic steps as illustrated in Fig 3.

There are a few fundamental challenges that had to be overcome in the fabrication process, which did not exist in either the switchable PG or polymer PG fabrication processes. First, we had to be able to create very high quality, uniform polymer PGs at high thicknesses (up to 18 individual layers for 8-10 μm thickness) This is essential to the creation of a uniform cell gap and can be achieved by very careful control of the polymer spinning and photopolymerization process. Removing the edge bead after the spinning process also improves uniformity.

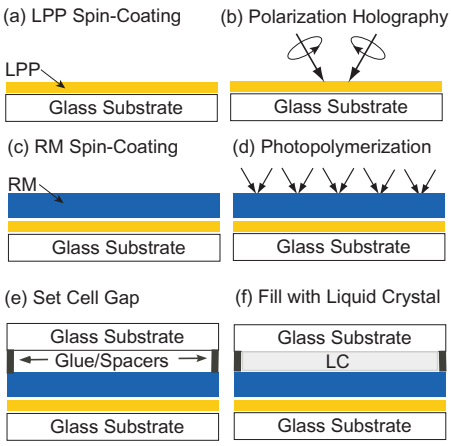

Figure 3. Basic fabrication steps for the BPG

3.3 Experimental Results

In our preliminary experiment we created BPGs of four different thicknesses. In each case the switchable layer was the same thickness, while the polymer layer thickness was increased by one full-wave retardation in each case. The first grating was made without a polymer layer, essentially yielding a PG of one full-wave retardation at 685 nm (due only to the switchable layer). The second grating exhibited one full-wave retardation due to the polymer layer, and another due to the switchable layer for an overall two-full wave retardation at 685 nm. The third and fourth gratings had three and four full-waves retardation respectively due to polymer layers and one-full wave from the switchable layer. In other words, for the first grating the $N = 1$ peak occurred at 685 nm, for the second grating the $N = 2$ peak lined up at the same wavelength, and the third and fourth gratings had peaks $N = 3$ and $N = 4$ at that same wavelength. The experimental spectra of each of these four gratings are shown in Fig. 4 All gratings were fabricated with a grating period of 15.8 μm.

By applying an external voltage each of the four peaks were tuned as shown in Fig. 4. The threshold voltage for the four gratings is 1.8 V, 2.4 V, 4 V, and 5.2 V respectively. These voltages are slightly higher than those of standard switchable LCPGs since a proportional amount of the applied voltage is dropped across the polymer layer.

4. THE BPG TUNABLE OPTICAL FILTER

We have constructed a tunable optical filter by stacking multiple BPGs in a Lyot-type configuration followed by a spatial filter (Fig. 5). We will first describe the fundametal concepts and governing equation of the BPG tunable optical filter, then we will discuss the advantages of a BPG filter over our previously introduced tunable optical filter created from standard switchable LCPGs.[30] We will characterize the the filter in terms of its full-width at half-maximum (FWHM), free-spectral-range (FSR), and the *finesse* (FSR/FWHM).

4.1 Theory

The general structure of the BPG tunable optical filter is described in Fig. 5. At least three BPGs of increasing thickness are stacked such that the optic axis of each is rotated with respect to each other in order to achieve proper separation of the orders. All but the zero order is then blocked using a spatial filter (which is illustrated in the most simple case as a lens and aperture immediately before a photodetector). The resulting transmittance (0th order transmittance) is a multiplication of the individual zero-order efficiencies and the losses due to Fresnel reflections and electrode absorption:

$$T(\lambda) = K^M \prod_{m=1}^{M} \eta_{0,m}(\lambda) = K^M \prod_{m=1}^{M} \cos^2\left(\frac{\pi \Delta n d_m}{\lambda}\right) \tag{5}$$

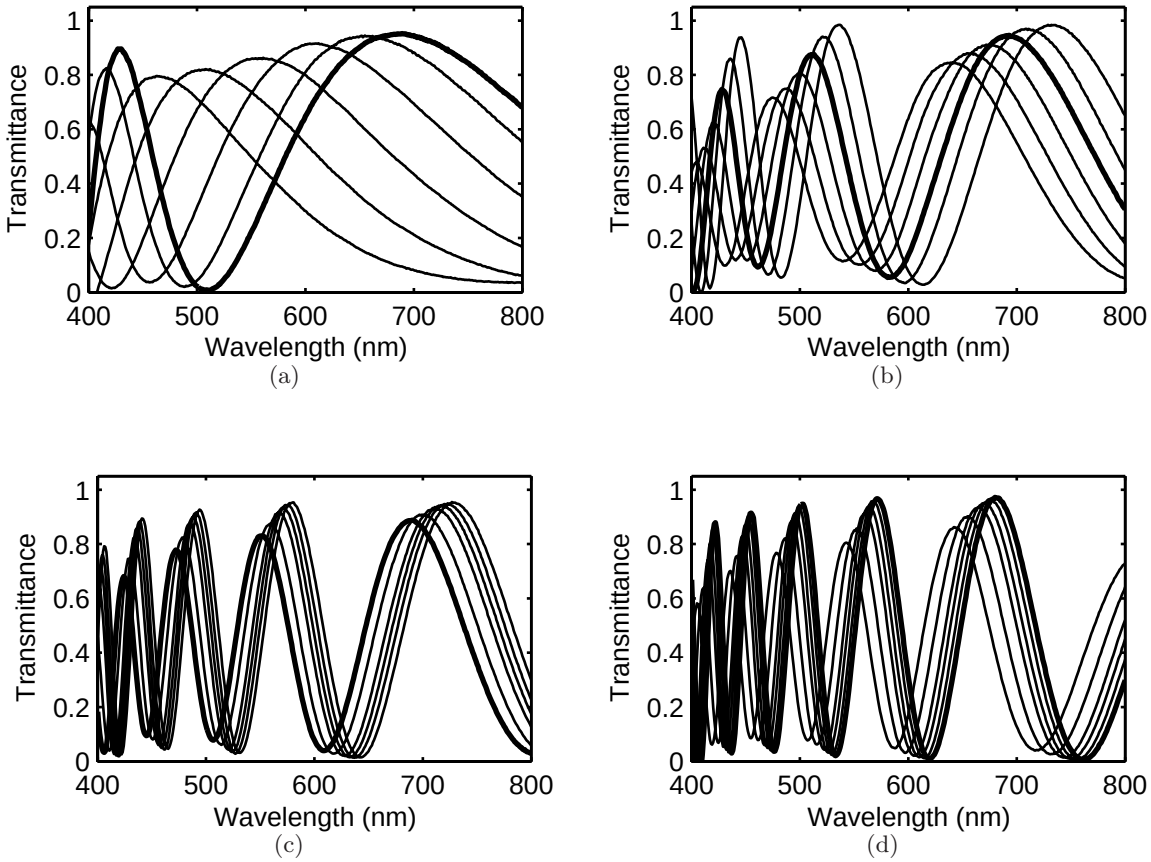

Figure 4. Experimental voltage-resolved spectra for the (a) One-full-wave, (b) Two-full-wave, (c) Three-full-wave, and (d) Four-full-wave BPGs. The boldface curve is at tuned such that the peak of interest ($N = 1, 2, 3$ and 4 respectively) is at the center wavelength (685 nm).

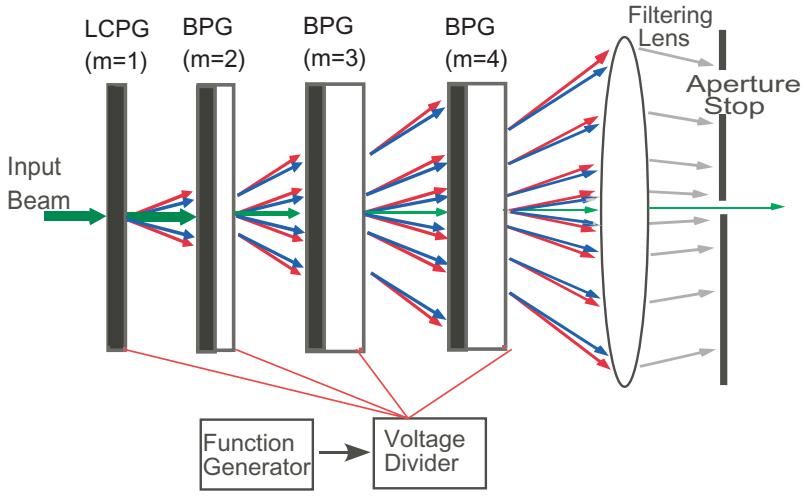

Figure 5. The basic BPG tunable optical filter structure showing individual gratings and the propagation of light through them. Note that in this paper we study three stages (M=3).

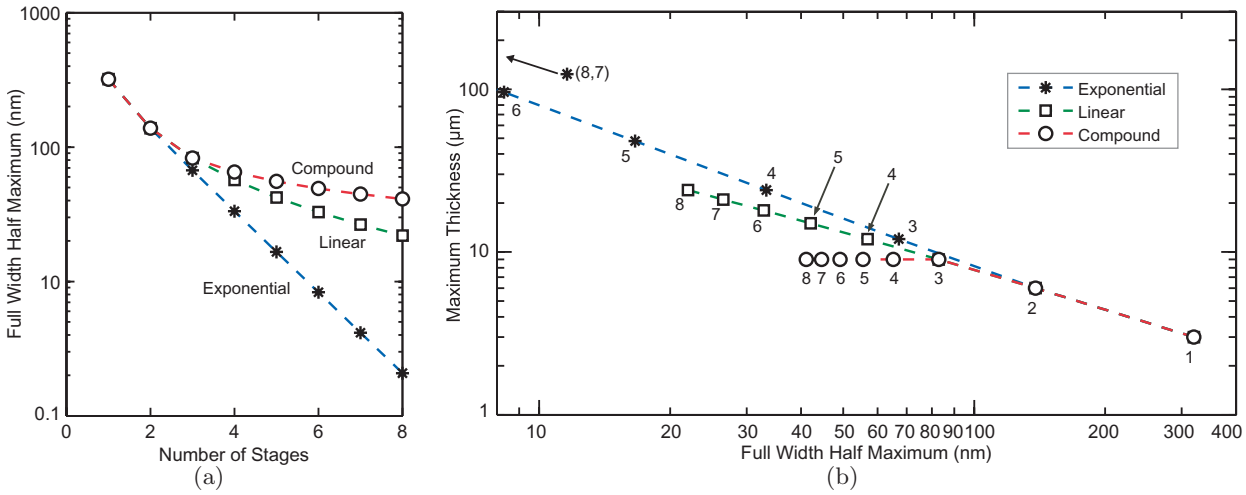

Figure 6. Simulated diffraction characteristics of LCPGs versus number of stages M: (a) Full-width at half-maximum and (b) Maximum required LCPG thickness and FWHM (numbers indicate M for each point)[30]

where M is the total number of stages, K is the combined transmittance of the substrates and electrodes within each stage, $\eta_{0,m}(\lambda)$ is the efficiency of stage m, and d_m is the LC layer thickness of grating m. Keep in mind that it is most accurate to consider $\Delta n \rightarrow \Delta n(V)$, which accomplishes the tuning effect. Given a design wavelength λ_0 and LC material, Eq. (2) can be employed to determine a minimum thickness required by setting $N = 1$. Note that the thinnest BPG must be at least thick enough to exhibit one full-wave retardation ($\Delta n d_1 \geq \lambda_0$), and would often be constructed as a conventional LCPG (without the polymer layer) in order to maximize its tuning range.

Previously we introduced three design possibilities or filter progressions involving the choice of d_m and M each exhibiting a trade-off between maximum required grating thickness and minimum possible FWHM (or maximum Finesse).[30] We described an exponential ($d = d_0 * 2^{(m-1)}$), linear ($d = d_0 * m$), and compound (first three gratings follow linear then the third grating is repeated) progression of grating thicknesses. As can be seen from the simulation plots in Fig. 6 we show that the optimum configuration is the exponential one since it yields the lowest FWHM with the fewest number of gratings. This is important since the absorption in the ITO and glass surfaces, although very small, can become significant if multiplied through many interfaces. For example, if a filter with 30 nm as the FWHM target was needed, it would require 4, 6, and and many more than 8 stages for the exponential, linear, and compound constructions respectively. Furthermore, each approach would require a maximum LC layer thickness of 25 μm, 15 μm, and 9 μm respectively. The central difficulty is that while the exponential approach leads to the fewest required stages, it demands the highest (by far) LC thickness. It is this limitation that we overcome here. As with all LC devices, large thicknesses (e.g. $d > 50$ μm) are difficult to work with because they tend to have slow response times and are prone to defects. Furthermore, a larger thickness imposes a large grating period (typically $\Lambda \geq 1.5d$). While this is usually achievable using holographic techniques, a large Λ leads to a small angle separating the zero- and first-orders, and restricts the numerical aperture of the tunable filter.

The other two important filter parameters we will consider are free-spectral-range (FSR) and *finesse*. FSR is a quantity that describes the distance to the next adjacent spectral peak and fundamentally this peak should occur at half the design wavelength (685 nm). However we must take into account the effects of dispersion which may cause this peak to occur at a slightly higher wavelength. Finesse is a quantity describing the ratio of FSR to FWHM and is therefore inversely proportional to FWHM and dependent upon the same design parameters.

The BPG tunable optical filter provides an elegant solution allowing us to take advantage of the increase in quality expected from the exponential filter while maintaining a thin switchable LC layer. Since a BPG can achieve the same properties as an LCPG with a thinner switchable layer, we can fabricate a very thick

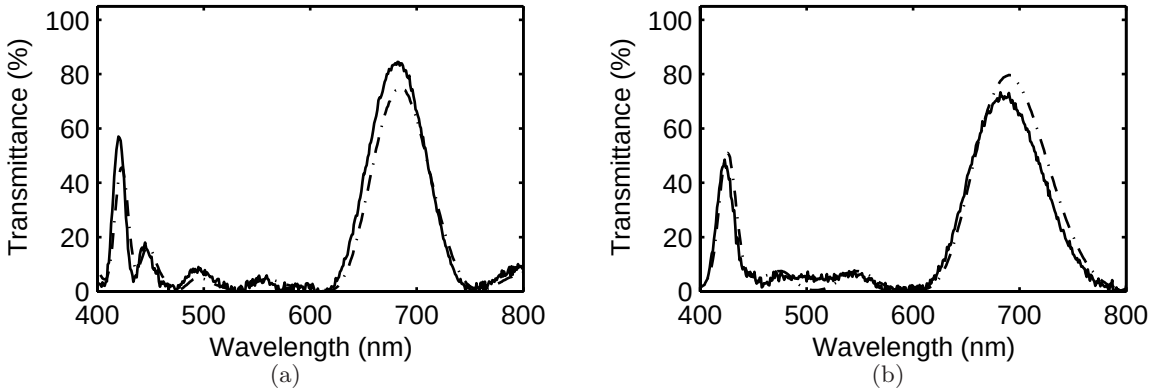

Figure 7. Experimental spectra (solid line) and predicted spectra (dashed line) of the (a) exponential progression filter, (b) linear progression filter

grating with a thin switchable layer which which ensures fast response times and fewer defects. Furthermore, we can maintain a relatively small grating period which leads to larger separation between the orders allowing for increased numerical aperture of the filter.

4.2 Preliminary Results

Using the gratings detailed in Sec. 3.3 and following the filter theory set forth in Sec. 4.1 two prototype filters were created, each composed of three gratings of increasing thicknesses. The first filter was constructed in the linear progression and the second using the exponential progression in order to verify the theoretical advantages of an exponential progression filter. The first filter consisted of the 1, 2, and 4 full-wave retardation grating and the second filter was constructed using a 1,2, and 3 full-wave retardation grating. Both filters were designed to have a maximum center wavelength at 685 nm. Note that when we characterize individual PGs we express the spectra in terms of *diffraction efficiency* which is a normalized term that describes the inherent diffraction behavior of a single PG and is directly related to Eq. 1. However the filter spectra are characterized in terms of their *transmittance* which is a true (un-normalized) measure including all substrate, interface, and grating effects. Fig. 7 shows both the predicted (multiplication of the 0-voltage spectra of the individual gratings) and experimental spectra for both the exponential and linear filters.

Both the linear and exponential filters behaved as predicted theoretically as shown by the spectra in Fig. 7. The linear progression filter exhibited a FWHM of $\sim$ 80 nm where as the exponential progression showed a FWHM of $\sim$ 64 nm. This means a modest decrease in FWHM which is consistent with theoretical predictions. The exponential progression filter showed a peak transmittance of approximately 84% as opposed to the 72% peak transmittance of the linear progression. This reduction in peak transmittance is due to the lower peak transmittance of the 3 full wave grating which must be initially biased to 2.6 V to reach the design wavelength. In general the peak transmittance is a multiplication of the transmittances of the individual gratings. Therefore it suffers from multiplicative absorption losses in each glass substrate leading to a lower maximum than any one individual grating. Both configurations showed very low noise and no significant side-lobes other than the secondary spectral peak just above 400 nm which is expected considering dispersion effects. This secondary peak is used to measure the FSR of the filter, which in this case is approximately 260 nm leading to a *finesse* of approximately 4 (in the exponential progression case). The tuning range for both is approximately 160 nm which is equivalent to one-full wave retardation at 685 nm (i.e. the thickness of the LC layer).

Electrical tuning of the filter is achieved by individual control of each polarization grating with an applied voltage. Depending on small fabrication variations, some of the stages may have to be initially biased so that the operational peak occurs at the design starting wavelength (in this case, 685 nm). This initial calibration results in a single bandpass region with maximum peak transmittance and minimum FWHM. This peak can then be tuned across the tuning range ($\sim$ 160 nm) by individually controlling the increase of applied voltage to each cell.

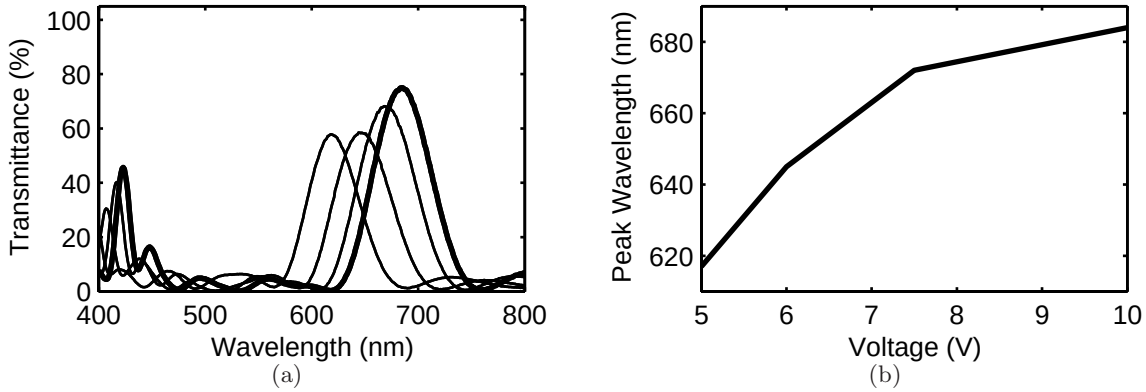

Figure 8. Experimental spectra of the (a) exponential progression filter, (b) linear progression filter, and (c) exponential filter tuning with applied voltage

Fig. 8(a) depicts the tuning of the exponential progression filter. In this case the highest applied voltages required to achieve the 67 nm shift shown in Fig. 8(a) are 2.0 V, 3,6 V, and 10 V for the 1,2, and 4 full-wave stages respectively. Fig. 8(b) shows the peak wavelength versus voltage characteristic of the filter where the voltage is that of the 4 full-wave stage. While the essential tuning function is clearly prominent, we notice a reduction in the peak transmittance as the voltage is applied. We anticipate that this is not a fundamental limitation, but rather due to a spatially non-uniform tilt profile of the LC director as a voltage is applied. We believe that photo-alignment materials and processing techniques that enable stronger anchoring strength will reduce this effect. Further investigation into the exact causes and possible solutions to this degrading effect is a primary focus of our future work.

In order to further improve on current results, we suggest the addition of more stages to the filter in the exponential progression. We have shown experimentally that the exponential progression is most favorable as long as we can keep the switchable layer thin (i.e. by implementing the BPG). However, we recognize that further optimization of materials and fabrication is required to optimize filter characteristics. In particular, we need to study effective methods of obtaining very uniform, predictable, and consistent cell gaps.

5. CONCLUSION

We have experimentally demonstrated a BPG tunable optical filter with a peak transmittance of 84% of unpolarized light, a FWHM of 64 nm, a tuning range of 160 nm, FSR of 260 nm, *finesse* of 4, and initial center wavelength of 685 nm. By applying modest voltages $\sim$20 V, we tuned the passband of the filter down to 525 nm, a tuning range of 160 nm . We introduce the Bilayer Polarization Grating for the first time and demonstrate that at least two complex anchoring conditions can be achieved with high quality: (i) a reactive mesogen PG aligning a switchable LC and (ii) a degenerate-planar anchoring surface with low pretilt enabling uniform orientation without defects of the switchable LC. We then apply the BPG to a tunable optical filter. Most critically, this is implemented with a polarization-independent approach without polarizers, and uses materials and construction with strong potential for low cost and small size implementations. We also experimentaly demonstrate the theoretical trade-offs between different filter configurations. We conclude that the BPG tunable optical filter shows properties ideal for use in compact, portable spectrometers and other low cost remote sensing systems.

ACKNOWLEDGMENTS

The authors gratefully acknowledge financial support from the National Science Foundation (grant ECCS-0621906).

REFERENCES

1. K. Rosfjord, R.A.Villalaz, and T. Gaylord, "Constant-bandwidth scanning of the Czerny Turner monochromator," *Applied Optics* **39**(4), pp. 568–572, 2000.
2. A. Kenda, W. Scherf, R. Hauser, H. Gruger, and H. Schenk, "A compact spectrometer based on a micromachined torsional mirror device," *Proceedings of IEEE Sensors* **3**, pp. 1312–1315, 2004.
3. A. Kutyrev, C.L.Bennett, S. Moseley, D. Rapchun, and K. Stewart, "Near infrared cryogenic tunable solid fabry-perot spectrometer," *Proceedings of SPIE* **5492**, pp. 1172–1179, 2004.
4. K. Hirabayashi, H. Tsuda, and T. Kurokawa, "A tunable polarization-independent liquid crystal Fabry-Perot interferometer filter," *Journal of Lightwave Technology* **11**(12), pp. 2033–2043, 1993.
5. B.Lyot, "Filter monochromatique polarisane et ses applications en physique solarie," *Annales d'Astrophysique* **7**(31), 1944.
6. H. Morris, C. Hoyt, P. Miller, and P. Treado, "Liquid crystal tunable filter raman chemical imaging," *Applied Spectroscopy* **50**(6), pp. 805–811, 1996.
7. A. Sneh and K. Johnson, "High-speed continuously tunable liquid crystal filter for [wdm] networks," *Journal of Lightwave Technology* **14**(6), pp. 1067–1080, 1996.
8. C. Ye, "Low-loss tunable filter based on optical rotatory dispersion," *Applied Optics* **45**(6), pp. 1162–1168, 2006.
9. I.Solc, "Birefringent chain filters," *Journal of the Optical Society of America* **55**(6), pp. 621–625, 1965.
10. B. Benkelfat, Q. Zout, and B. Vonouze, "Low-voltage continuous tunable hybrid filter for tailored optical-bandwidth operation," *IEEE Photonics Technology Letters* **16**(4), pp. 1098–1100, 2004.
11. J. Evans, "Solc birefringent filter," *Journal of the Optical Society of America* **48**(3), pp. 142–145, 1958.
12. J. Evans, "The birefringent filter," *Journal of the Optical Society of America* **39**(3), pp. 229–242, 1949.
13. C. Chen, C. Pan, C. Hsieh, Y. Lin, and R. Pan, "Liquid-crystal-based terahertz tunable lyot filter," *Applied Physics Letters* **88**(10), p. 101107, 2006.
14. H. Xianyu, S. Faris, and G. Crawford, "In-plane switching of cholesteric liquid crystals for visible and near-infrared applications," *Applied Optics* **43**(26), pp. 5006–5015, 2004.
15. J. W. McMurdy, G. P. Crawford, and G. D. Jay, "Monolithic microspectrometer using tunable ferroelectric liquid crystals," *Applied Physics Letters* **89**(081105), 2006.
16. J. W. McMurdy, J. N. Eakin, and G. P. Crawford, "Vertically aligned deformed helix ferroelectric liquid crystal configuration for reflective display device," *SID Symposium Digest* **37**, pp. 677–680, 2006.
17. T. Vo-Ding, D. Tokes, M. Wabuyele, M. Martin, J. Song, R. Jagannathan, E. MIchaud, R. Lee, and X. Pan, "A hyperspectral imaging system for in vivo optical diagnostics," *IEEE Engineering in Medicine and Biology Magazine* , pp. 40–49, 2004.
18. M. Martin, M. Wabuyele, K. Chen, P. Kasili, M. Panjehopour, M. Phan, B. Overholt, G. Cuningham, D. WIlson, R. DeNovo, and T. Vo-Ding, "Development of an advanced hyperspectra imaging (hsi) system with applications for cancer detection," *Anals of Biomedical Engineering* **34**, pp. 1061–1068, 2006.
19. Z. Liu, Q. Li, J. Yan, and Q. Tang, "A novel hyperspectral medical sensor for tongue diagnosis," *Sensor Review* **27**(1), pp. 57–60, 2007.
20. L. Nikolova and T. Todorov, "Diffraction efficiency and selectivity of polarization holographic recording," *Optica Acta* **31**, pp. 579–588, 1984.
21. F. Gori, "Measuring stokes parameters by means of a polarization grating," *Optics Letters* **24**(9), pp. 584–586, 1999.
22. J. Tervo and J. Turunen, "Paraxial-domain diffractive elements with 100% efficiency based on polarization gratings," *Optics Letters* **25**(11), pp. 785–786, 2000.
23. C. Oh and M. J. Escuti, "Numerical analysis of polarization gratings using the finite-difference time-domain method," *Physical Review A* **76**, p. in press, 2007.
24. J. Eakin, Y. Xie, R. Pelcovits, M. D. Radcliffe, and G. Crawford, "Zero voltage freedericksz transition in periodically aligned liquid crystals," *Applied Physics Letters* **85**(10), pp. 1671–1673, 2004.
25. W. M. Jones, B. L. Conover, and M. J. Escuti, "Evaluation of projection schemes for the liquid crystal polarization grating operating on unpolarized light," *SID Symposium Digest* **37**, pp. 1015–1018, 2006.

26. M. J. Escuti, C. Oh, C. Sanchez, C. W. M. Bastiaansen, and D. J. Broer, "Simplified spectropolarimetry using reactive mesogen polarization gratings," *Proceedings of SPIE* **6302**, p. 630207, 2006.
27. G. Crawford, J. Eakin, M. Radcliffe, A. Callan-Jones, and R. Pelcovits, "Liquid-crystal diffraction gratings using polarization holography alignment techniques," *Journal of Applied Physics* **98**, p. 123102, 2005.
28. S. M. Kelly, "Anisotropic networks," *Journal of Materials Chemistry* **5**(12), pp. 2047–2061, 1995.
29. D. J. Broer, J. Bovern, and G. Mol, "In-situ photopolymerization of oriented liquid-crystalline acrylates," *Makromol. Chem.* **190**, pp. 2255–2268, 1989.
30. E. Nicolescu and M. J. Escuti, "Polarization-independent tunable optical filters based on liquid crystal polarization gratings," *Proceedings of the SPIE - Optics and Photonics Conference SPIE* **6654**(665405), 2007.
31. M. J. Escuti and W. M. Jones, "A polarization-independent liquid crystal spatial-light-modulator," *Proceedings of the SPIE - Optics and Photonics Conference* **6332**(63320M), 2006.
32. M. Schadt, H. Seiberle, and A. Schuster, "Optical patterning of multi-domain liquid-crystal displays with wide viewing angles," *Nature* (381), pp. 212–215, 1996.
33. H.-S. Kwok, V. G. Chigrinov, H. Takada, and H. Takatsu, "New developments in liquid crystal potoaligning by azo-dyes," *IEEE/OSA Journal of Display Technology* **1**(1), pp. 41–50, 2005.
34. I. Dozov, D. Stoenescu, S. Lamarque-Forget, P. Martinot-Lagarde, and E. Polossat, "Planar degenerated anchoring of liquid crystals obtained by surface memory passivation," *Applied Physics Letters* **77**(25), pp. 4124–4126, 2000.